buildings

MDPI

Article

Modern Design Methods on Optimised Novel Aluminium Profiles

Eva Marinopoulou [1], Konstantinos Daniel Tsavdaridis [2,*] and Evangelos Efthymiou [1]

[1] Institute of Metal Structures, Department of Civil Engineering, Faculty of Engineering, Aristotle University of Thessaloniki, 54124 Thessaloniki, Greece
[2] Department of Engineering, School Science & Technology, City, University of London, Northampton Square, London EC1V 0HB, UK
* Correspondence: konstantinos.tsavdaridis@city.ac.uk

Abstract: Within the framework of optimisation of structural elements, in the last years, significant activity has been demonstrated towards developing new sectional designs beyond standardised forms aiming to combine aesthetic innovation, material efficiency, and weight over stiffness, together with structural reliability and manufacture cost savings. Moreover, in terms of sustainability performance, as material-weight reduction leads to less carbon emissions from production to installation processes, the pursuit of suitable materials that can correspond to this challenge becomes imperative. In this context, aluminium is lightweight and corrosion resistant, but due to its low elastic modulus, an increased cross-sectional stiffness is required. In this paper, 16 previously optimised aluminium cross-section profiles are presented and analysed using the finite element analysis software ABAQUS. The obtained ultimate compression resistances were compared with the predictions made in accordance with Eurocode 9, the direct strength method (DSM), and the continuous strength method (CSM). The percentage of difference of these design methods with respect to FE results is depicted. The outcomes point out the vagueness in accuracy of the prediction methods, particularly in reference to stocky or slender cross-sections.

Keywords: optimised sections; aluminium; modern methods; design calculation; topology optimisation; Eurocode 9; slenderness

Citation: Marinopoulou, E.; Tsavdaridis, K.D.; Efthymiou, E. Modern Design Methods on Optimised Novel Aluminium Profiles. *Buildings* **2022**, *12*, 1904. https://doi.org/10.3390/buildings12111904

Academic Editor: André Rafael Dias Martins

Received: 18 September 2022
Accepted: 4 November 2022
Published: 7 November 2022

1. Introduction

Aluminium cross-sections are present in an increasing number of structural applications in the civil engineering domain. They can be found in lightweight structures, such as trusses and domes, as an appropriate substitute of steel sections, being significantly heavier. The material's corrosion resistance enables its use in harsh conditioned environments, such as offshore structures that are exposed to humidity and corrosive substances. Aluminium also offers a design flexibility through the extrusion process, which can be useful when a specific aesthetic or architectural design is intended.

Aluminium alloys' relatively low elastic modulus can be balanced out through the design of complex cross-sections, with geometries able to produce large moments of inertia, resulting in higher cross-sectional stiffness values, EI [1]. Structural optimisation is a powerful tool towards this scope, since it enables the design of robust components that maintain a low weight through incorporating an optimal geometry and material distribution with regards to particular loading conditions. According to Mei et al. [2], structural optimisation can fit into four categories: size, shape, topology, and multi-objective optimisation. Topology optimisation, which is addressed herein, refers to the interaction between nodes or joints that comprise a structural member [2]. The optimal design is therefore produced through the removal of unnecessary members and parts of a cross-section that, given a specific loading, do not contribute to the stress distribution.

Aluminium is an appropriate material for such a use since it can be quite versatile from a geometry standpoint. A variety of shapes can be produced: complex geometries can be manufactured through extrusion, and thus the cross-sectional design is not constrained to conventional shapes and dimensions.

After its initial introduction from Bendsøe and Sigmund [3], the spatial distribution of material that occurs during topology optimisation was investigated by many researchers [4,5]. One of the first applications of optimised cross-sectional design on thin-walled beam sections was conducted by Kim and Kim [6]. In 2019, Tsavdaridis et al. introduced various novel aluminium section beam and column profiles with unique topologies [1]. Such optimal design approaches could serve as examples to future similar studies since they combine the innovative spirit of the topology optimisation technique with construction potential and engineering intuition.

While exceling in novelty, geometrically complex cross-sections are hard to incorporate into the standardised design procedure Eurocodes offer. Interaction between the members that form the cross-section shall be accounted for, and thus the need for more inclusive methods of behaviour prediction has emerged. The continuous strength method (CSM) was developed by Gardner et al. [7–13] for stainless and carbon steel members, and it caters to this exact need: its scope is to replace the conventional cross-section classification that the European standards (EC3, EC9) [14] suggest, with a relationship that actively accounts for the cross-section's slenderness effect in the member's deformation capacity. According to Gardner et al. [10–13], the prediction method has produced increases in the compressive and bending resistances of metals that range from 5% to 20%.

CSM for aluminium structures has been investigated by Ashraf and Young [15] and Su et al. [16–19]. Su et al. [16–19] investigated CSM's application on aluminium alloys through a series of experimental data as well as proposing some additions to better fit aluminium members. Slenderness plays a significant role, since when a cross-section is considered slender, it fails from buckling prior to yielding, and thus it cannot deploy any benefits arising from strain hardening. Additionally, plasticity in aluminium alloy structures is addressed by Ampatzis et al. [20] and Georgantzia et al. [21], who demonstrated that the most precise ultimate resistances that employed aluminium's plasticity were produced by both CSM and the plastic hinge method.

Optimised cold-formed, thin-walled sections do not solely comprise flat-plated elements. Thus, the effective width method is most of the time insufficient to fully capture the geometry's effects on the member's resistance. Aiming to simplify the calculation of the elastic buckling stress and the effective properties of optimised steel sections, Schafer and Peköz developed the direct strength method (DSM) in 1998 [22–25]. They evaluated its performance in the member resistance estimation through comparing its results with AISI specifications. For some years now, DSM has been officially part of the design specifications featured in Appendix A of the AISI's North American specifications [26,27]. Additionally, the DSM has also been included in the Australian/New Zealand design specifications [25] in Section 7 of AS/NZS 4600:2018 [28]. However, the literature provided above refers to cold-formed steel sections. Zhu and Young slightly altered the DSM equations, aiming to expand the prediction method to aluminium members as well [29,30]. They produced a DSM alteration for aluminium members, which was shown to be congruent with the experimental and numerical results.

While topology optimisation is a promising domain in structural applications, there is still some progress to be made in terms of connecting the outputs (products) to the corresponding design guidelines. Eurocode 9 (EC9) covers a variety of standard cross-sections; however, novel forms that could provide increased design flexibility and aesthetic alternatives mentioned above are currently unaccounted for. Consequently, the scope of the herein presented research is to structurally validate novel aluminium sections derived through topology optimisation application, aiming to add reliable alternative profiles that conform to current codification and methodology adopted in this field [14].

In particular, eight stub columns were examined under concentric compression, and the corresponding limit state of EC9-clause 6 was investigated. Comparison of the FE results and the design guidelines of EC9 was also conducted. In this regard, numerical analyses were performed on aluminium beams of complex cross-sectional shapes. Initially, small modifications were carried out on the beam profiles each time, aiming to understand the effect of each parameter on the overall structural performance of the member. Each modified profile was also evaluated in accordance with the EC9 framework and then compared with the obtained analysis outcome. In this study, CSM was also considered as an approach to address post-yielding material behaviour, specifically in non-slender sections. CSM results are herein compared to both the FEA outcomes and the EC9 design formulae.

This paper attempted to highlight the need for an initial integration of complex geometries to the EC9 design guideline in a standard manner that can be feasible for a designer to follow, without having to rely solely on heavy FEM analyses. The general concept is the evolution of the current design range into a wider spectrum that involves novel, optimal designs that can produce innovative structural applications and reduce the weight without compromising the capacity.

2. Materials and Methods

Figure 1a presents four profiles derived from structural topology optimisation, recently developed by Tsavdaridis et al. [1]. The proposed dimensions suggest the desired ratios to be kept constant during sizing. Considering that aluminium has a rather low elastic modulus in comparison to steel, an increased cross-sectional moment of inertia is required to mitigate failure risks. Complex cross-section shapes could provide that, without necessarily using large amounts of additional material, thus increasing the structure's weight.

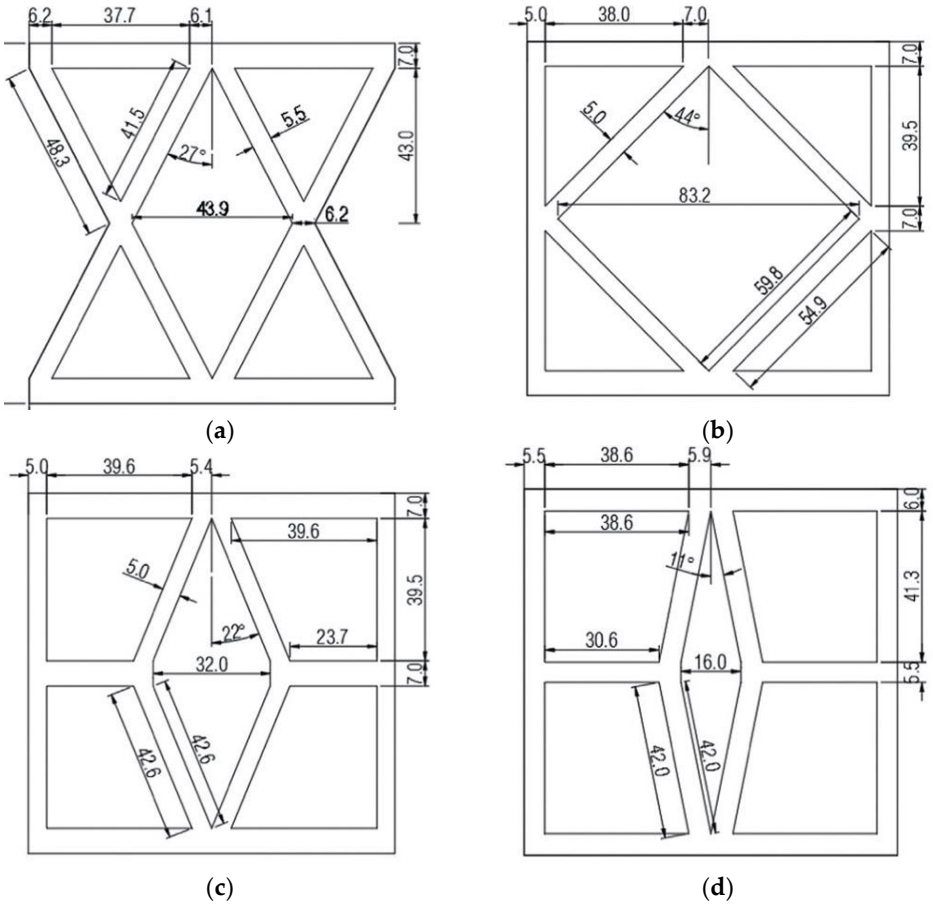

Figure 1. (**a**–**d**) Novel cross-section shapes (optimised). All cross-sections are 100 mm × 100 mm.

For the purpose of this study, finite element software Abaqus CAE [31] was employed to simulate the behaviour of the optimised aluminium alloy stub columns. Before conducting any numerical analysis, two stub column models (a simple rectangular and an optimised one) were validated against experimental work found in the literature [17], as depicted in Figure 2. The models used for the purpose of the validation studies were the SV1, SV2, and SV3 (SV—section validation). SV1, which is referenced in [1,17] as H70 × 55 × 4.2C-R, is a rectangular cross-section-analysed by Tsavdaridis et al. [1] and experimentally investigated by Su et al. [17]. SV2 and SV3, referenced in [1] as S1 and S2, are optimised cross-sections proposed by Tsavdaridis et al. [1]. Material properties and dimensions can be seen in Table 1. The boundary conditions of the columns were constrained by reference points located at the centroid of each section, on the upper and lower end. The lower end was fixed, while the upper end had one degree of freedom, the axial displacement.

A linear eigenvalue buckling analysis was conducted to model the geometric imperfections on the columns. According to the literature [1,32–34], geometrical imperfection was modelled with a value of 0.5 mm, accounting for the 10% of the extruded profile's thickness. As a general rule, cross-sectional thickness can vary up to 5%, while parts thinner than 5 mm can produce deviations up to 10%. Hollow extruded profiles vary in this manner because of the extrusion process [35].

In a free mesh consisting of 8 mm sized triangular elements, C3D10 was used, as can be seen in Figure 2b. The stress distribution plots for the validation sections, SV2 and SV3, are presented in Figure 2c,d, respectively. The contour plots refer to the entire columns, as well as to the middle cross-section. The validation models were compared with S1 and S2, which were obtained from the literature [1]. For the static non-linear second-order analysis, Abaqus' Riks method was employed. The validation models were evaluated in comparison to the experimental specimen in terms of stress–strain curve, as shown in Figure 3.

Table 1. Material properties and dimensions of each model.

Cross-Section	B (mm)	H (mm)	t_w (mm)	t_f (mm)	L (mm)	Material	ρ (ton/mm^3)	E (GPa)	ν	f_p (MPa)	f_{max} (MPa)	ε_{max}
SV1	70	54.9	4.08	4.08	209.9	Al 6063-T6	2.7×10^{-9}	70	0.3	160	195	0.106
SV2	100	100	5.00	5.00	300.0	Al 6063-T6	2.7×10^{-9}	70	0.3	160	195	0.106
SV3	100	100	7.50	5.00	300.0	Al 6063-T6	2.7×10^{-9}	70	0.3	160	195	0.106

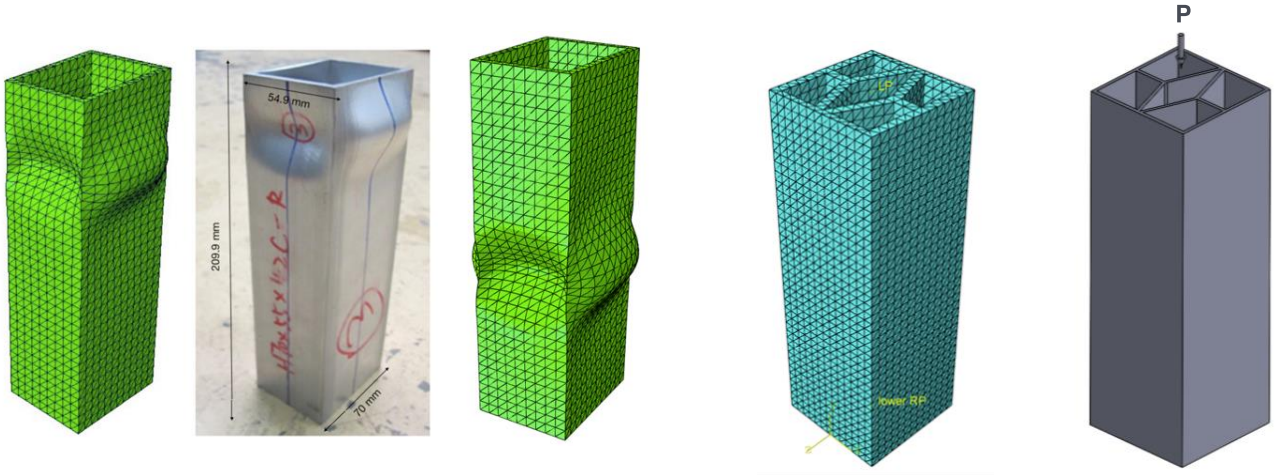

Figure 2. *Cont.*

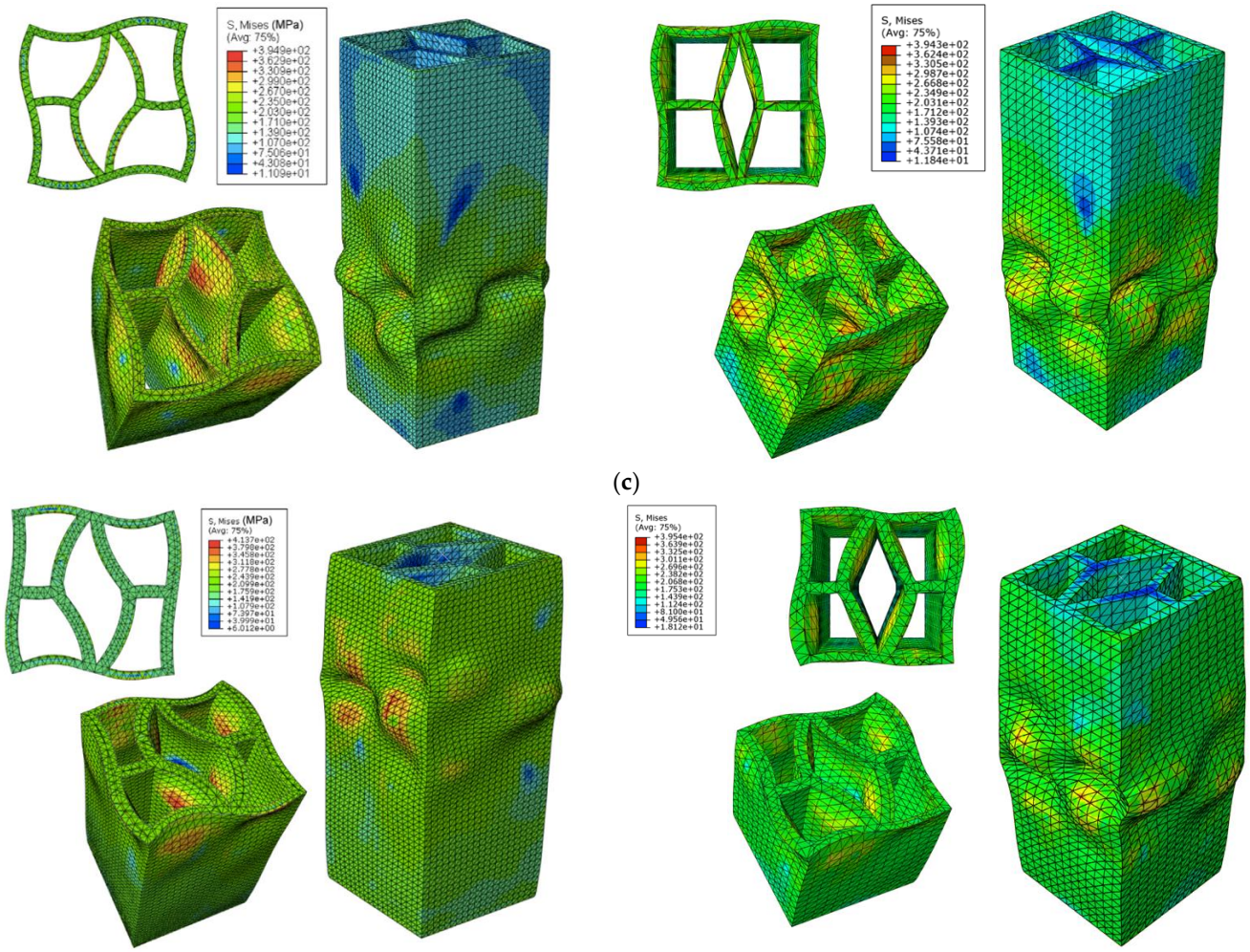

(**c**)

(**d**)

Figure 2. Validation analyses: (**a**) rectangular H70 × 55 × 4.2C-R cross-section [1] (**left**), SV1 (**right**); (**b**) mesh, load, and boundary conditions (same across all models); (**c**) S1 optimised cross-section [1] (**left**), SV2 (**right**); (**d**) S2 optimised cross-section [1] (**left**), SV3 (**right**).

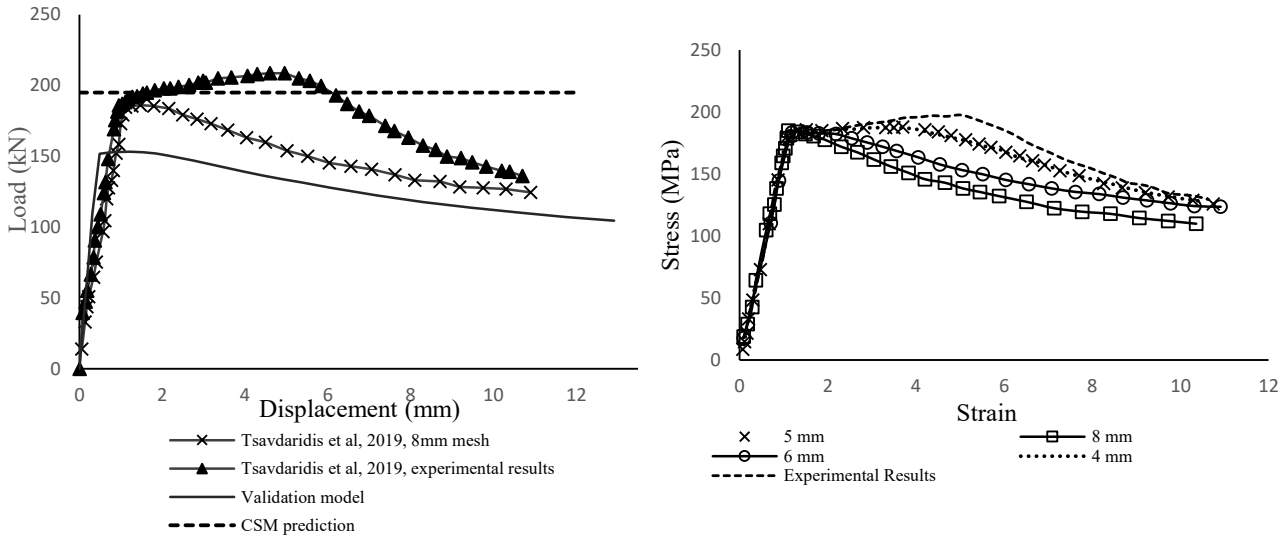

(**a**)

Figure 3. *Cont.*

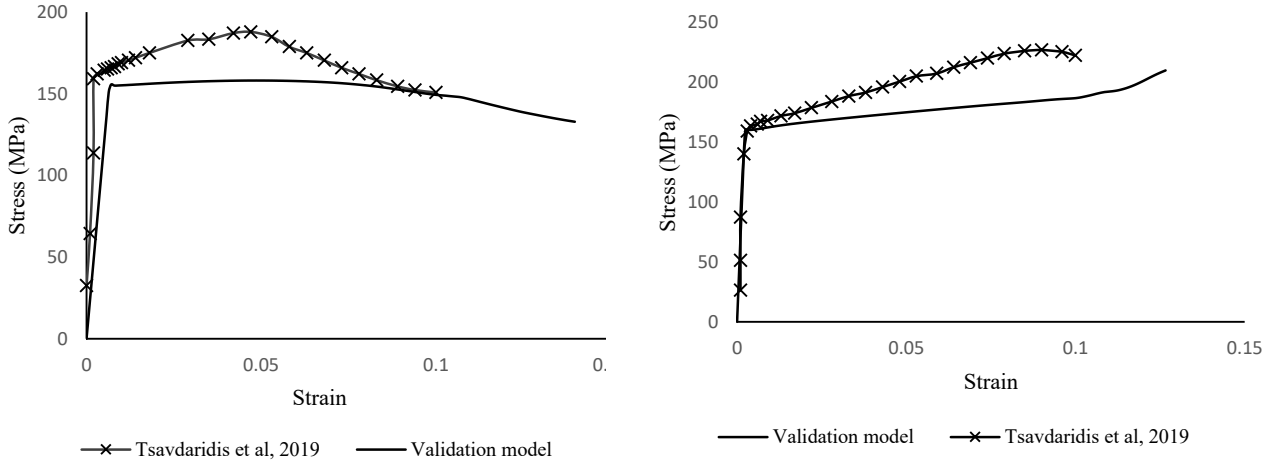

(**b**)

Figure 3. Validation analyses: (**a**) load–displacement curves—SV1 (**left**), load–displacement curves for various mesh sizes [1] (**right**). (**b**) Stress–strain curve—SV1 (up), stress–strain curve—SV2 (down).

For the CSM predictions, the equations that were used, as given by Su et al. [16], are provided below. Initially, the cross-section slenderness, λ_p, was determined. The cross-section slenderness is a non-dimensional form acquired by the square root of the ratio of the yield stress f_y to the elastic buckling stress σ_{cr} of the cross-section, as can be seen in Equation (1). All the cross-sections investigated in this paper were non-slender, since their cross-section slenderness, λ_p, was lower than 0.68. In this study, the elastic buckling stress was calculated through a formula acquired from Seif and Schafer [36], as shown in Equation (2). Thereafter, the cross-section deformation capacity needs to be determined, which is expressed as the ratio of the CSM-predicted level of strain, ε_{csm}, to the yield strain, ε_y. This is given by a prediction provided in Su et al. [16], which is accurate for aluminium alloy profiles, both stocky and slender, as shown in Equation (3). In addition, the strain hardening slope was calculated by Equation (4), which employs the yield and ultimate strength as well as the yield and ultimate strain, f_y, f_u, ε_y, and ε_u, respectively. C2 is the proportion of ultimate strain and is assumed to be 0.5, which corresponds to an adequately accurate σ-ε curve. Consequently, the limiting CSM predicting ultimate capacity is given by Equation (5).

Cross-sectional slenderness, CSM:

$$\lambda_p = \sqrt{f_y/\sigma_{cr}}, \tag{1}$$

Elastic buckling stress:

$$\sigma_{cr} = k_b \frac{\pi^2 E}{12(1-\nu^2)} \left(\frac{t}{b}\right)^2 \tag{2}$$

where k_b = 4 for h/b = 1

Stocky cross-sections: Cross-sectional deformation capacity:

$$\frac{\varepsilon_{csm}}{\varepsilon_y} = \frac{0.25}{\lambda_p{}^{3.6}}, \text{ but less than min} \left\{15, \frac{0.5\varepsilon_u}{\varepsilon_y}\right\}, \tag{3}$$

Slender cross-sections: Cross-sectional deformation capacity:

$$\frac{\varepsilon_{csm}}{\varepsilon_y} = \left(1 - \frac{0.222}{\lambda_p{}^{1.05}}\right) \cdot \frac{1}{\lambda_p{}^{1.05}}$$

Strain hardening slope:

$$E_{sh} = \frac{f_u - f_y}{C_2\varepsilon_u - \varepsilon_y} = \frac{f_u - f_y}{0.5\varepsilon_u - \varepsilon_y} \tag{4}$$

CSM limiting stress:

$$f_{csm} = f_y + E_{sh}\left(\varepsilon_{csm} - \varepsilon_y\right) \geq P_{csm} = Af_{csm} \tag{5}$$

DSM predictions were calculated using the adjusted equations for aluminium cross-sections, provided by Zhu and Young [37,38]. In similarity with CSM, the cross-section slenderness λ_c is a non-dimensional form determined from the critical buckling load P_{cr} and the yield load P_y, as can be seen in Equation (6). P_{cr} and P_y are given in Equations (7) and (8), respectively. The DSM resistance for aluminium, non-welded columns, as proposed by Zhu and Young [37,38], is given in Equation (9). It is significant to note that the equations' adjustments covering aluminium members, compared to the original relations that refer to steel sections, are rather minor. For more details on these modifications, the reader can refer to [37,38].

Cross-sectional slenderness values according to the DSM:

$$\begin{aligned} \lambda_c &= \sqrt{P_y / P_{cre}} \\ \lambda_l &= \sqrt{P_{ne} / P_{crl}} \end{aligned} \tag{6}$$

where P_{cre} is the critical elastic buckling load,

$$P_{cre} = \frac{\pi^2 EA}{\left(l_{eff}/r\right)^2} \tag{7}$$

and P_{crl} is the critical elastic local buckling load of the cross-section, obtained from Gardner et al. [39].

Yield load:

$$P_y = f_y \cdot A \tag{8}$$

DSM prediction resistance: P_{DSM} = min (P_{ne}, P_{nl})

$$\begin{aligned} P_{ne} &= \begin{cases} \left(0.658^{\lambda_c^2}\right) \cdot P_y \; for \; \lambda_c \leq 1.5 \\ \left(\frac{0.877}{\lambda_c^2}\right) \cdot P_y \; for \; \lambda_c \geq 1.5 \end{cases} \\ P_{nl} &= \begin{cases} \left(0.658^{\lambda_c^2}\right) \cdot P_{ne} \; for \; \lambda_l \leq 0.713 \\ \left[1 - 0.15 \cdot \left(\frac{P_{crl}}{P_{ne}}\right)^{0.3}\right] \cdot \left(\frac{P_{crl}}{P_{ne}}\right)^{0.3} for \; \lambda_l > 0.713 \end{cases} \end{aligned} \tag{9}$$

EC9 predictions are calculated for the compression limit state of clause 6.2.4, when the cross-sections are not slender, meaning that they fail due to yielding and not buckling. For cross-section S1, which is class 3, the minimum resistance between buckling, Equation (10), and compression, Equation (11), is assumed.

Compression limit state resistance:

$$N_{c,Rd} = Af_0 / \gamma_{M1} \tag{10}$$

Buckling limit state resistance:

$$N_{b,Rd} = \kappa\chi Af_0 / \gamma_{M1} \tag{11}$$

where γ_{M1} = 1.10, and κ, χ are provided by EC9 formulae and characteristic values in accordance with the member's buckling class (either A or B).

The stub column models of the parametric study were square hollow sections with various thicknesses; square hollow sections with a central circular opening, as developed

by Kim and Kim [5]; and optimised cross-sections developed by Tsavdaridis et al. [1]. The geometries of the cross-sections can be seen in Figure 4a–d. The alloy was aluminium 6063-T6, with an elastic modulus of 70 GPa; a density of 2.7 gr/mm^3; and a yield and ultimate strength of 160 and 195 MPa, respectively. The Poisson's ratio was 0.3, and the ultimate strain was 0.106. The column dimensions can be found in Table 2. The material was class A according to Table 3.2b of EC9, while the columns ranged from Class 1 to 4, EC9-6.1.1.4 [13]. The column boundary conditions were constrained by reference points located at the centroid of the section, on the upper and lower end. The lower end was fixed, while the upper end had one degree of freedom, the axial displacement. A free mesh consisting of 8 mm sized triangular elements, C3D10, was used. Like in the validation studies, an eigenvalue buckling analysis was conducted first to model the geometric imperfections on the column. As mentioned above, as in [1,32–34], geometrical imperfections were modelled with values that account for the 10% of the profiles' thicknesses, which was the most unfavourable scenario.

Table 2. Detailed profile dimensions.

Cross-Section	B (mm)	H (mm)	t_w (mm)	t_f (mm)	L (mm)	R
Q1	100	100	5	5	300	-
Q2	100	100	7	7	300	-
Q3	100	100	7	5	300	-
Q4	100	100	5	7	300	-
Q5	100	100	3	3	300	-
K1	100	100	7	7	300	15
K2	100	100	7	7	300	20
K3	100	100	7	7	300	30
K4	100	100	7	7	300	35
K5	100	100	3	3	300	10
S1	100	100	4	4	300	-
S2	100	100	5	5	300	-
S3	100	100	6	6	300	-
S4	100	100	7	7	300	-
S5	100	100	3	3	300	-
S6	100	100	2	2	300	-

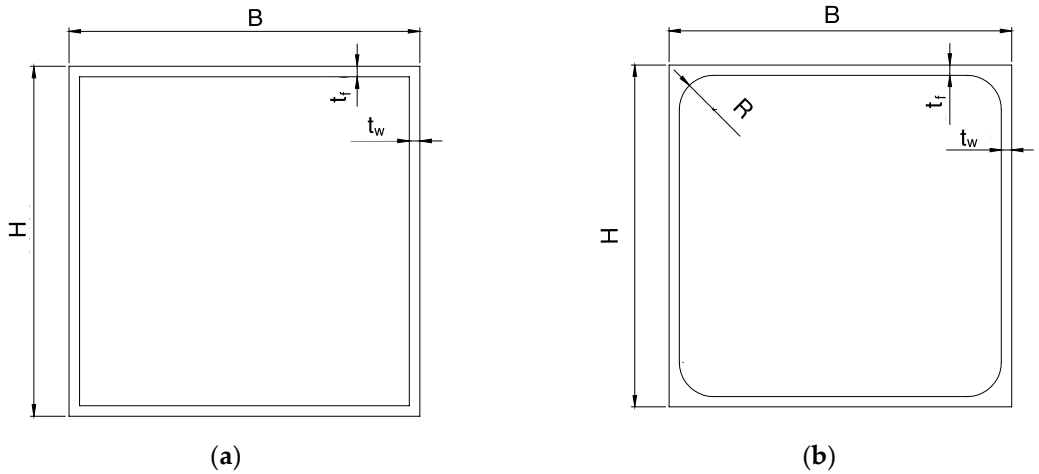

(**a**) (**b**)

Figure 4. *Cont.*

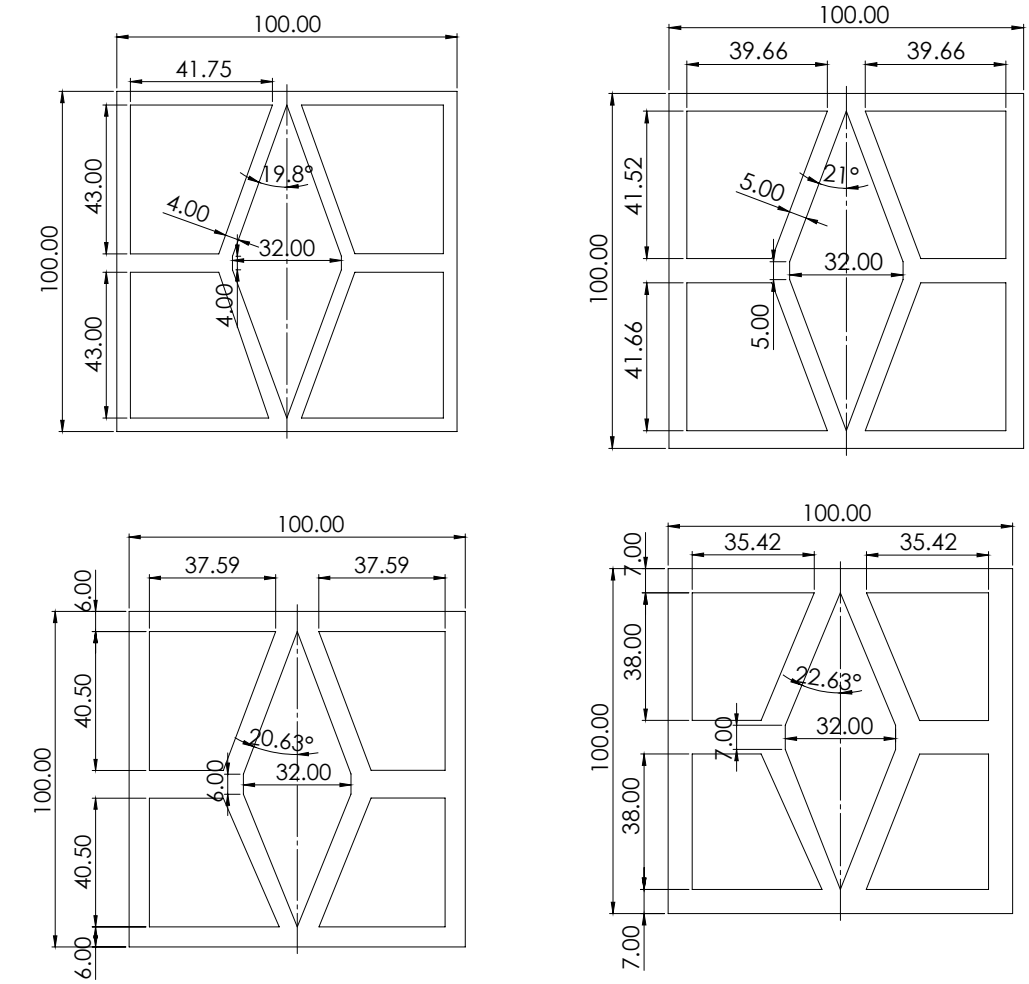

(**c**)

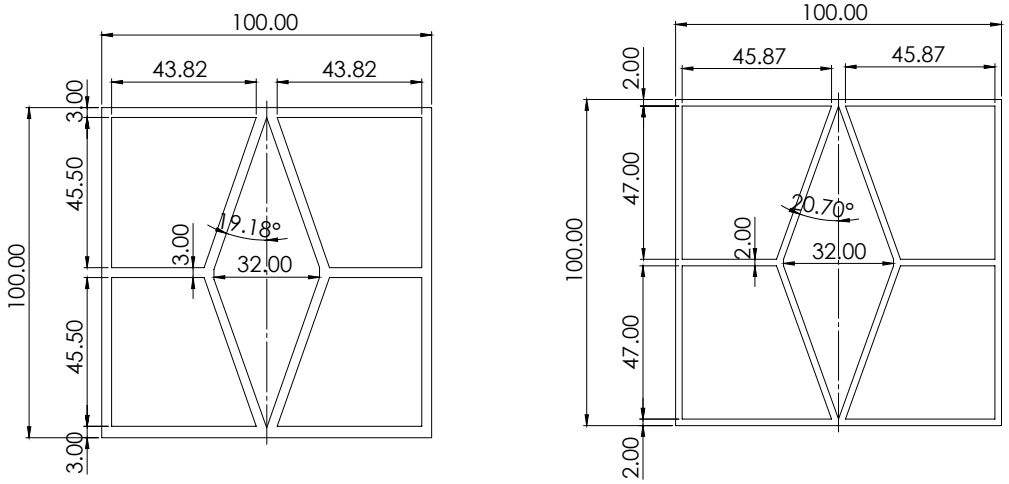

(**d**)

Figure 4. Cross-sectional geometries: (**a**) non-slender Q1–Q4; (**b**) non-slender K1–K4, (geometries based [5]); (**c**) non-slender S1–S4 (developed [1]); (**d**) slender S5–S6 (developed [1]). All cross-sections were 100 mm × 100 mm.

3. Results

The results of the parametric analyses are depicted in Figure 5a–c for the Q, K, and S-type cross-sections, respectively, while the results of the slender cross-section analyses can be seen in Figures 5d and 6a,b, which are the load-displacement curves for each stocky and slender column, respectively. The maximum loads obtained from EC9, FEA, CSM, and DSM can also be found in Table 3 and Figures 7 and 8.

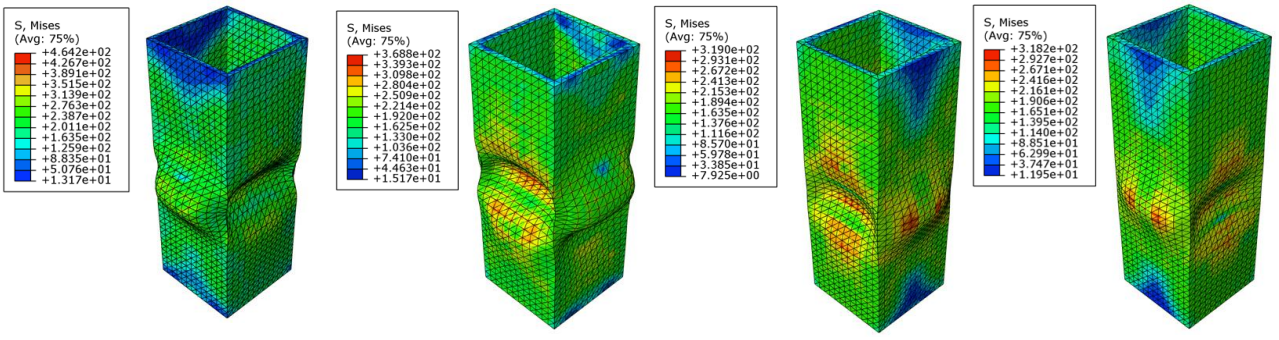

(**a**)

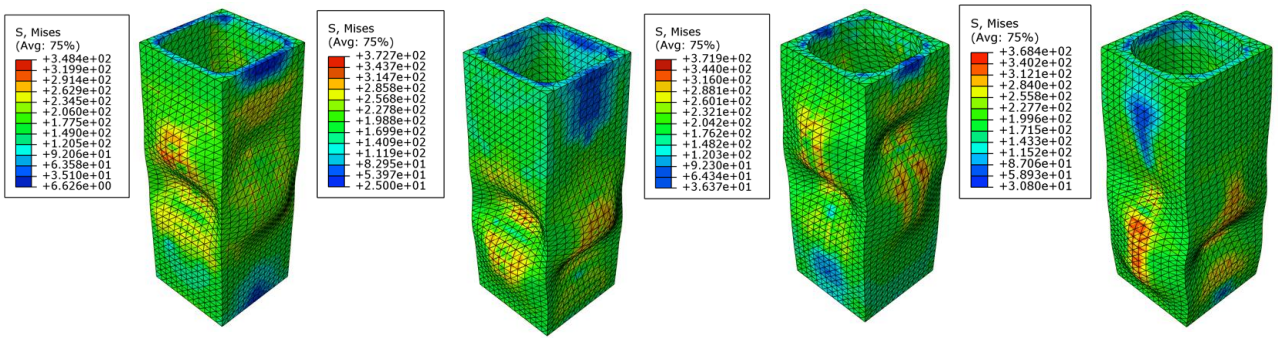

(**b**)

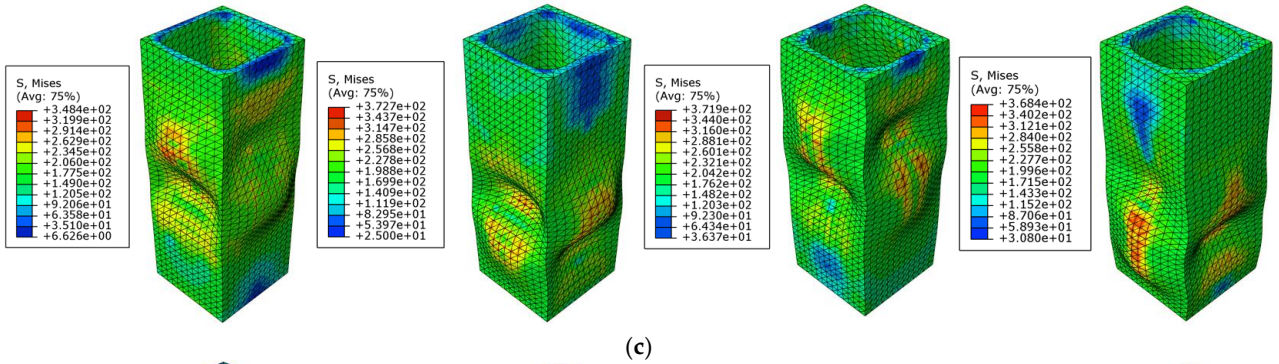

(**c**)

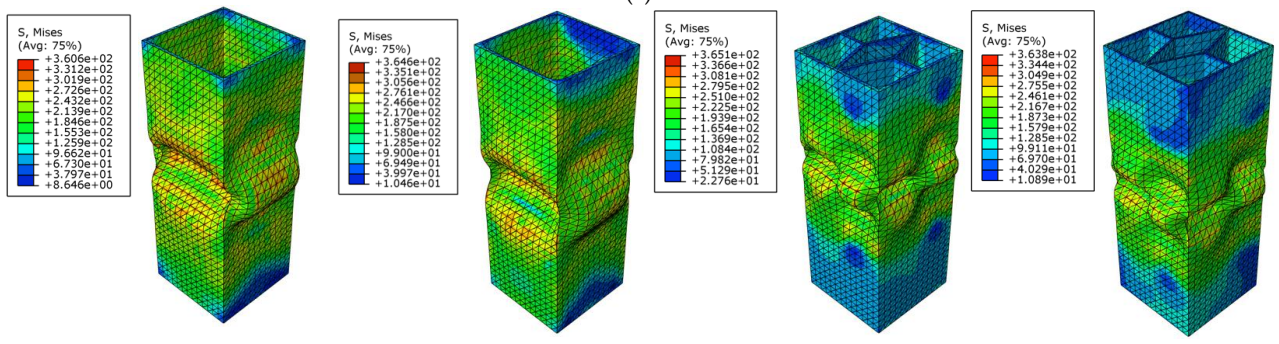

(**d**)

Figure 5. Stress distribution plots: From left to right: (**a**) Q1–Q4 stocky cross-sections; (**b**) K1–K4 stocky cross-sections; (**c**) S1–S4 stocky cross-sections; (**d**) Q5, K5, and S5–S6 slender cross-sections.

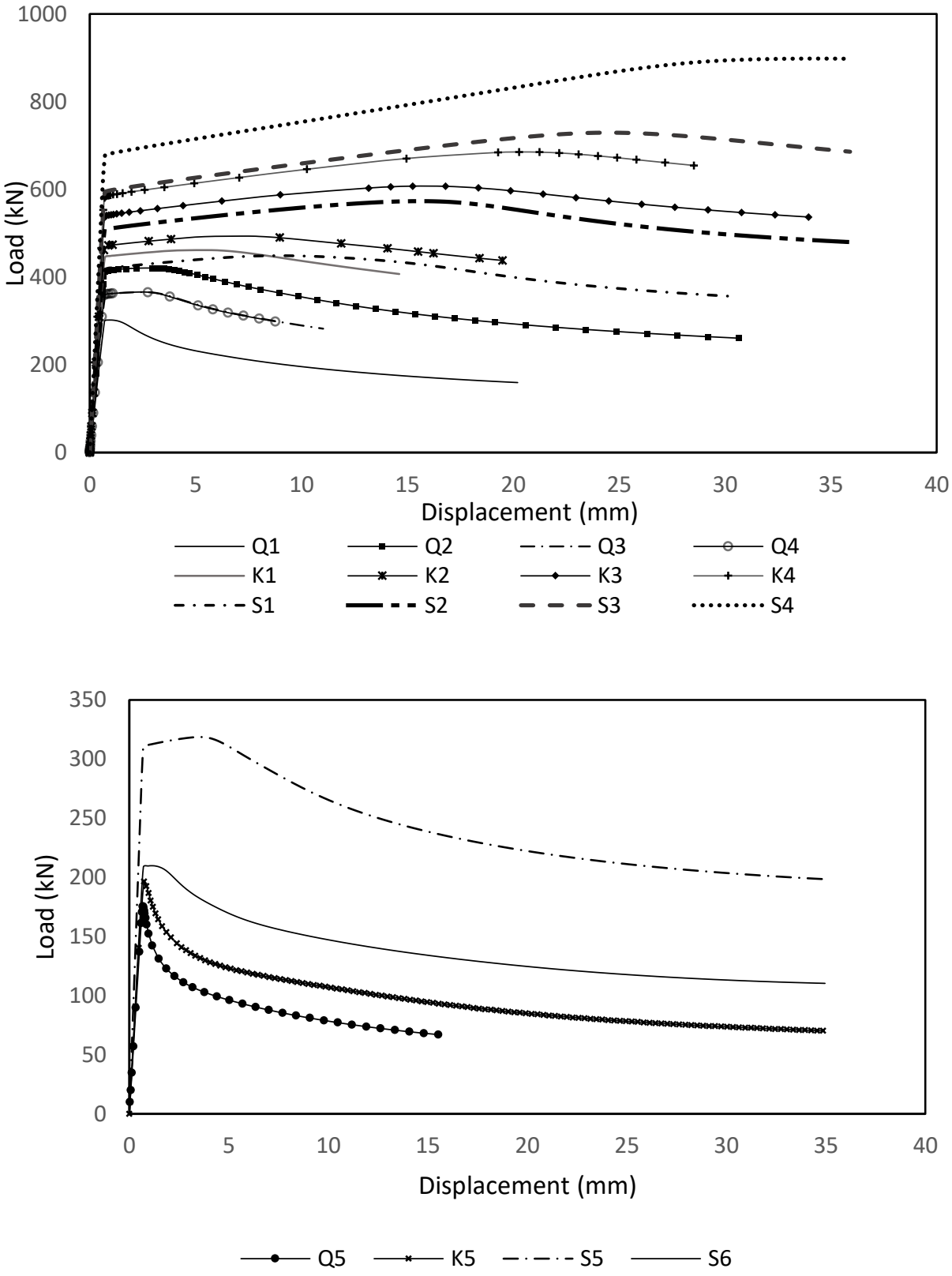

Figure 6. Load–displacement curves for each stocky column (FEA).

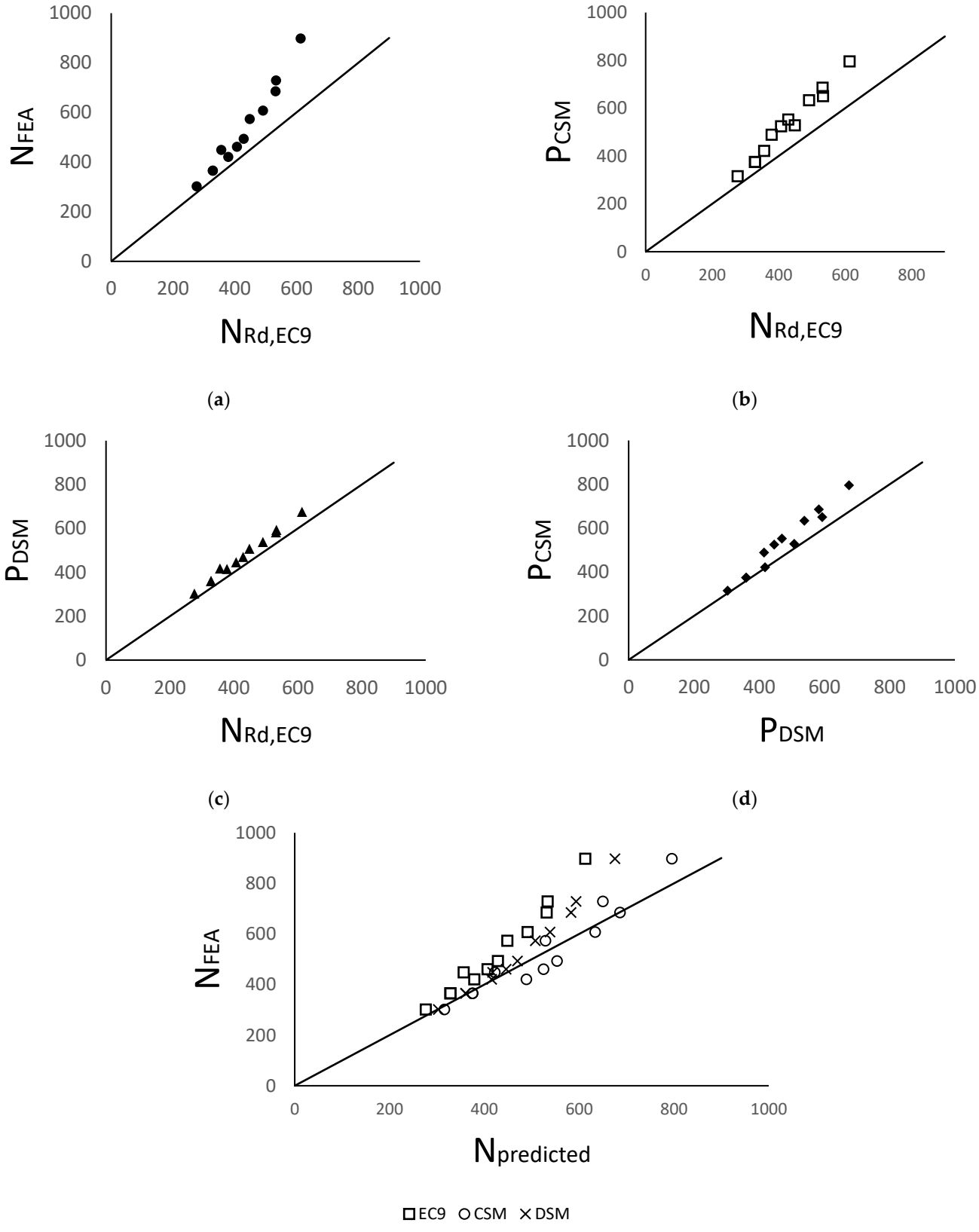

Figure 7. Stocky cross-sections: Comparison between the maximum compressive resistances obtained from (**a**) FEA vs. EC9; (**b**) CSM vs. EC9; (**c**) DSM vs. EC9; (**d**) CSM vs. DSM; (**e**) FEA-obtained values vs. predictions from different methods, EC9, CSM, and DSM.

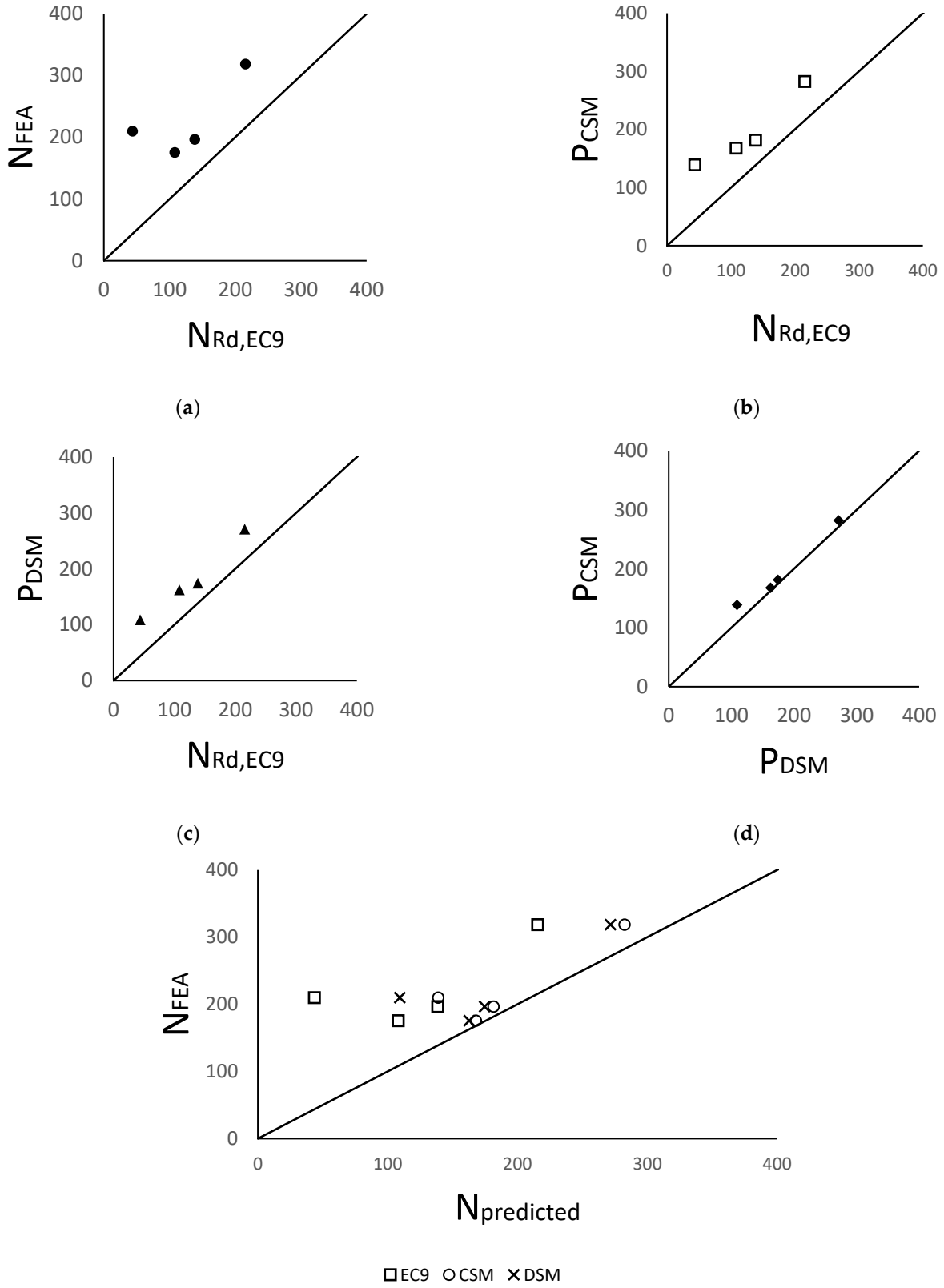

Figure 8. Slender cross-sections: Comparison between the maximum compressive resistances obtained from: (**a**) FEA vs. EC9; (**b**) CSM vs. EC9; (**c**) DSM vs. EC9; (**d**) CSM vs. DSM; (**e**) FEA-obtained values vs. predictions from different methods, EC9, CSM, and DSM.

Table 3. Ultimate strength as calculated by EC9, CSM, and DSM formulae and as obtained from FEA. Increase/decrease percentages from one cross-section to another are also presented. Strength values are given in kN.

Cross-Section	N_{Rd} EC9		N_{Rd} FEA		P_{CSM}		P_{DSM}	
Q1	276.4		302.1		315.6		303.1	
Q2	378.8	*37.1%*	420.7	*39.3%*	488.8	*54.9%*	415.4	*37.0%*
Q3	328.7	*−13.2%*	365.8	*−13.0%*	375.4	*−23.2%*	360.5	*13.2%*
Q4	328.7	*0.0%*	365.9	*0.0%*	375.4	*0.0%*	360.5	*0.0%*
Q5	108.1	*23.8%*	175.4	*26.1%*	168.0	*39.9%*	162.7	*23.8%*
K1	406.9		461.4		525.1		446.2	
K2	428.7	*5.4%*	493.5	*6.9%*	553.3	*5.4%*	470.2	*5.4%*
K3	491.1	*14.6%*	607.5	*23.1%*	633.9	*14.6%*	538.6	*14.6%*
K4	531.7	*8.3%*	685.3	*12.8%*	686.2	*8.3%*	583.1	*8.3%*
K5	138.5	*−32.9%*	196.5	*−34.5%*	181.6	*−38.5%*	174.7	*28.4%*
S1	356.6		448.8		422.1		417.7	
S2	448.6	*25.8%*	573.2	*27.7%*	529.0	*25.3%*	507.5	*21.5%*
S3	533.5	*18.9%*	729.3	*27.2%*	654.0	*23%*	593.6	*17.0%*
S4	613.1	*14.9%*	898.2	*23.2%*	796.0	*22.4%*	675.7	*13.8%*
S5	215.5	*−64.8%*	318.7	*−64.5%*	282.5	*−64.5%*	271.6	*−59.8%*
S6	43.6	*−79.8%*	209.9	*−34.1%*	139.0	*−50.8%*	109.2	*−59.8%*

3.1. Stocky Cross-Sections

3.1.1. Comparison of FEA against EC9

When comparing the FEA results with the EC9 calculations, the Q-type cross-sections demonstrated a stable percentage of difference between 9 and 11%. The K- and S-type cross-sections demonstrated larger differences, ranging from 13% to 29% and 26% to 46%, respectively. The differences increased as the radius increased on the K-type cross-sections, while on the S-type cross-sections, the percentage growth was caused by the larger thicknesses. Thus, from the current analysis, it can be concluded that the stockier members (or in the case of K-sections, the members with higher radiuses) developed a large difference between the FEA results and the EC9 predictions. This was an expected outcome, since EC9 does not factor in the material's strain hardening effects. Moreover, it can be observed from FEA results in Figure 6 that less slender cross-sections demonstrated higher strain hardening in the post-elastic region.

Zhu et al. [18] observed that for aluminium columns, the difference between FEA results and EC9 predictions is around 6–29%, with the FEA-predicted resistance always being higher. The cross-section thicknesses varied from 0.4 to 2 mm, while the differences decreased as the thicknesses increased. Su et al. [17] examined aluminium rectangular stocky (EC9 Class 1–3) hollow sections under compression, and the results showed that the experiments produced around 1–15% difference in resistance values. Equally, the resistances obtained from the tested specimens were greater than the EC9 estimations. Georgantzia et al. [40] observed that FEA results on aluminium angle stub columns of Classes 1, 2, and 3 differed by a mean value of 11% with EC9 predictions. On Class 4 cross-sections, the differences were up to 22%. The literature [37,40] agrees with these results, since the derived resistances differ by percentages up to 30%. Through the analyses conducted for this study, it was observed that there was not a clear pattern on how FEA and EC9 percentages of differences change when the cross-section's thickness was modified.

As Figure 6a suggests, stocky cross-sections demonstrate higher strain hardening in the post-elastic region. Slender cross-sections are less likely to develop strain hardening since they tend to experience local buckling prior to yielding [16].

Steel members that have also been examined under compression tests in the literature [9] have demonstrated differences between 5 and 20%, with the FEA or the experimental value always being higher than the EC9 prediction.

3.1.2. Comparison of CSM against FEA and EC9

According to the outcomes of the FEA conducted for the present study, it was not particularly clear if CSM predictions were more accurate as the cross-sectional thickness increased or decreased. The Q- and S-type cross-sections developed larger differences as the thickness increased, while the K-type cross-sections demonstrated the reverse effect. In specific, K4, which had the largest radius, produced the same compression resistance for CSM and FEA. CSM and FEA results diverged up to 14% on the slenderer, Q-type columns. CSM predictions overestimated the compression resistance on Q- and K-type cross-sections and underestimated it on the S-type cross-sections.

In comparison to EC9, the developed deviations were higher, specifically reaching up to 30%. The CSM predictions were always higher. In this case, it was observed that an increase in thickness led to an increase in deviation. This was true for Q- and S-type cross-sections, while on the K-type cross-sections, there was a stable difference percentage of 29% maintained throughout K1–K4. The explanation behind this similarity in values along K1–K4 is worth mentioning. P_{csm} was in direct relation to the thickness-to-width ratio, (t/b), while N_{Rd} was proportional to the cross-sectional area. Moreover, both formulae contained the material input, in forms of the yield stress, elastic modulus, and/or yield strain, as can be seen in Equations (1)–(7). The thickness-to-width ratio was kept constant for the K-type cross-sections, since the only factor changing between one another was the radius' value. This led to a constant cross-sectional slenderness, λ_p, and deformation capacity $\varepsilon_{csm}/\varepsilon_y$, and thus a constant CSM limiting stress, f_{csm}. Consequently, both for CSM and EC9, the only modified parameter between K1 and K4 was the cross-sectional area, which led to this stable difference percentage between the two methods' predictions. However, FEA results did not indicate any direct proportionalities of this sort. The Q-type cross-sections Q3 and Q4 produced an equal compression resistance according to both CSM and FEA. This was expected since Q3 and Q4, when loaded centrally as in the present study, were the same because of their symmetrical geometry.

In specific, for S-type cross-section geometries, CSM was found as precise since it only deviated by a slight 3–4%. As indicated in Table 3, an increase in thickness from S3 to S4 resulted in a N_{Rd} growth of 23%, as measured in FEA. CSM also estimated the percentage at 23%, while EC9 estimated only at 15%. When switching from S1 to S2 cross-sections, both CSM and EC9 provided accurate enough estimations, although as the thickness increased and the cross-sections became stockier, EC9 was less able to predict a precise percentage value. On the contrary, CSM was not that accurate in estimating the increase percentages on the K-type cross-sections. For example, while FEA suggested a N_{Rd} increase of 23% from K2 to K3 cross-sections, CSM only estimated a 14% increase. From section K3 to K4, the FEA-obtained increase was 13%, while the CSM-provided increase was 8%, and thus the convergence between $N_{Rd,K1\text{-}FEA}$ and $P_{K1\text{-}csm}$ might be random. EC9 predictions were almost identical to CSM's for the increase percentage on the K-type cross-section, meaning that both CSM and EC9 did not entirely capture the effect of the changing radius on the ultimate compressive resistance. It is worth noting that EC9 predicted the Q-type cross-sections in a very precise manner, since the maximum deviation it produced was a slight 2%. CSM, on the other hand, did not perform as well, since it estimated relatively large differences of values up to 17%.

In the literature, a stable pattern seems to appear between CSM and FEA estimations. It was observed that CSM predictions underestimated the cross-section's compression resistance in comparison to FEA results. In specific, Su et al. [16] found that the experimental

ultimate compression resistance was around 17% larger than the CSM estimation when slenderness λ_p was less than 0.3. However, Su et al. [17] also found that for various SHS cross-sections and especially for those with slenderness values over 0.4, the experimental compression resistance was lower than the CSM approach. The deviations formed between the two methods, as developed in the present study, can be seen in Table 3. The slenderness values for each column are presented on Table 4, where it can be observed that λ_p was always higher than 0.35. Zhu et al. [30] reported that for channel sections, which failed due to buckling, the CSM prediction was lower than the experimental resistance.

Table 4. CSM (λ_p) and DSM (λ_c, λ_l) slenderness values for each column.

Cross-Section	λ_p	**Cross-Section**	λ_p	**Cross-Section**	λ_p
Q1	0.50	K1	0.36	S1	0.63
Q2	0.36	K2	0.36	S2	0.50
Q3	0.50	K3	0.36	S3	0.42
Q4	0.50	K4	0.36	S4	0.36
Q5	1.25	K5	0.84	S5	0.84
				S6	1.25
Cross-Section	λ_c	**Cross-Section**	λ_c	**Cross-Section**	λ_c
Q1	0.08	K1	0.08	S1	0.10
Q2	0.08	K2	0.08	S2	0.10
Q3	0.08	K3	0.08	S3	0.10
Q4	0.09	K4	0.09	S4	0.10
Q5	0.08	K5	0.08	S5	0.09
				S6	0.08
Cross-Section	λ_l	**Cross-Section**	λ_l	**Cross-Section**	λ_l
Q1	0.45	K1	0.31	S1	0.58
Q2	0.31	K2	0.31	S2	0.45
Q3	0.45	K3	0.31	S3	0.37
Q4	0.45	K4	0.31	S4	0.31
Q5	0.79	K5	0.79	S5	0.79
				S6	1.21

Regarding steel members, Afshan et al. [9] proved that the experimental ultimate compressive resistance was around 9% higher than the CSM prediction.

3.1.3. Comparison of DSM against FEA and EC9

Comparing FEA results to the DSM estimations, it was firstly observed that the DSM predictions were always lower than the FEA-acquired resistances, and therefore the DSM is a safe approach. The ultimate loads of the Q-type cross-sections deviated less from the FEA results by using the DSM rather than the CSM, as Table A1 (Appendix A) suggests. K1 and K2 were better estimated using the DSM; however, K3 and K4, which were the stockiest two among the K-type cross-sections, were more accurately approached with CSM. All S-type cross-section resistances were more precisely predicted using CSM. Thus, it can be concluded that between the two methods, CSM is a better approach for stockier cross-sections, while DSM is more suitable for members with lower cross-sectional thicknesses that are, however, still not considered slender. When referring to a better approach, it is hereby meant that the resistance value differs slightly from the FEA result.

3.2. Slender Cross-Sections

Figure 6a,b clearly shows the different response stocky and slender cross-sections demonstrated, having the same loading and boundary conditions. Both the maximum yield stress and the post-yielding behaviour differed. The yield point of the slender cross-sections was substantially lower, while the plastic regions of the two cross-section types were also quite different: It is evident that for the slender cross-sections, strain hardening barely existed. This might have been true for some of the stocky cross-sections as well, especially for those with low thicknesses, but for most of the models, a significant amount of strain hardening took place.

4. Discussion

Demand for a wider range of design options calls for an initial integration of novel geometries to Eurocode 9 (EC9). Until now, such geometries can only be employed after being meticulously analysed through FEM. Thus, while topology optimisation creates favourable structural conditions, the lack of a standardised design guidelines is another obstacle for the designer.

CSM is a strain-based prediction method that has been widely mentioned in the literature. This study attempted to evaluate whether it could be employed to estimate the structural performance of non-standard shaped aluminium cross-sections, on the basis of the accuracy of the predictions. The DSM is a prediction method that simplifies the calculation of the ultimate resistance of optimised sections and has already gained momentum regarding steel members. However, its use has been limited to aluminium cross-sections.

The comparison of the ultimate compressive resistance values derived by the FEM, CSM, DSM, and EC9 for 12 different cross-sections indicated the lack of a clear pattern in the predictions. The parametric analysis showed that neither the EC9 nor CSM and DSM can fully capture the effect of the thickness or geometry change on the ultimate strength. However, the CSM and DSM were proven to be more accurate for the novel cross-section geometry studied in this project (S-type) in comparison to EC9. Furthermore, the results obtained from the analyses of the present study did not clearly denote whether either of the prediction methods are more accurate on stocky or slender cross-sections, which indicates the need for further research in the field.

Author Contributions: Conceptualization, K.D.T. and E.M.; methodology, K.D.T. and E.M.; software, E.M. validation, K.D.T. and E.M.; formal analysis, E.M.; investigation, E.M., K.D.T. and E.E.; data curation, E.M., K.D.T. and E.E.; writing—original draft preparation, E.M.; writing—review and editing, E.M., K.D.T. and E.E.; visualization, E.M.; supervision, K.D.T. and E.E.; project administration, K.D.T. All authors have read and agreed to the published version of the manuscript.

Funding: This research received no external funding.

Data Availability Statement: The data can be requested by the authors.

Conflicts of Interest: The authors declare no conflict of interest.

Appendix A

Tables A1 and A2 of the Appendix show the differences between the three methods in terms of ultimate compression resistances. Figure A1 contains the cross-sectional diagrams displaying the stress distribution of each stocky column type, plotted for the maximum load increment. Figure A2a–c are three evaluative graphs of the CSM, DSM, and EC9 which demonstrate the differences each one delivers in comparison to the FEA results.

The DSM produced results which were more closely related to EC9's predicted values, in comparison to the CSM. The highest deviation percentage was 30% for CSM, while it was only 17% on the DSM. A total of 9 out of the 12 cross-sections differed by 10% from the EC9 estimated resistances, which showed a pattern. The resistances of the S-type cross-sections were in better accordance with EC9 when the cross-sectional thickness was increased.

Figure A1 clearly shows that while EC9 estimations were relatively stable across all slenderness values, there were large deviations among DSM predictions. Cross-sections with the same slenderness value demonstrated differences in the error percentage, and thus there was no indication of a direct relationship between the slenderness value and the estimations' accuracy. This observation became particularly apparent in the S-type cross-sections, which demonstrated highly unstable deviations, while the K- and Q-type cross-sections showed somewhat identical percentages throughout the members.

Looking at Table A2, it can be concluded that the CSM delivered the most accurate prediction for the maximum resistance value of the slender cross-sections. It was also clear that the maximum deviation between the estimations and the FEA results were found in S5 and S6. This indicates that the interaction between the members of the complex geometries cannot be captured in the prediction methods. However, the CSM and DSM produced considerably more accurate results in comparison to EC9. This was of course expected, since EC9 is the most conservative approach between these three methods.

Table A1. Stocky cross-sections: comparison between the maximum compressive resistance values: ultimate load ratio and percentage deviation between two methods.

Cross-Section	$\frac{N_{FEA}}{P_{CSM}}$	$\frac{N_{FEA}}{N_{Rd,EC9}}$	$\frac{P_{CSM}}{N_{Rd,EC9}}$	$\frac{P_{DSM}}{N_{Rd,EC9}}$	$\frac{N_{FEA}}{P_{DSM}}$
Q1	0.96	1.09	1.14	1.10	1.00
Q2	0.86	1.11	1.29	1.10	1.01
Q3	0.97	1.11	1.14	1.10	1.01
Q4	0.97	1.11	1.14	1.10	1.02
K1	0.88	1.13	1.29	1.10	1.03
K2	0.89	1.15	1.29	1.10	1.05
K3	0.96	1.24	1.29	1.10	1.13
K4	1.00	1.29	1.29	1.10	1.18
S1	1.06	1.26	1.18	1.17	1.07
S2	1.08	1.28	1.18	1.13	1.13
S3	1.12	1.37	1.22	1.11	1.23
S4	1.13	1.46	1.30	1.10	1.33
Cross-Section	**CSM-FEA**	**FEA-EC9**	**CSM-EC9**	**DSM-EC9**	**FEA-DSM**
Q1	4%	9%	14%	10%	0%
Q2	14%	11%	29%	10%	1%
Q3	3%	11%	14%	10%	1%
Q4	3%	11%	14%	10%	2%
K1	12%	13%	29%	10%	3%
K2	11%	15%	29%	10%	5%
K3	4%	24%	29%	10%	13%
K4	0%	29%	29%	10%	18%
S1	−6%	26%	18%	17%	7%
S2	−8%	28%	18%	13%	13%
S3	−12%	37%	22%	11%	23%
S4	−13%	46%	30%	10%	33%

Table A2. Slender cross-sections: comparison between the maximum compressive resistance values: ultimate load ratio and percentage deviation between two methods.

Cross-Section	$\frac{N_{FEA}}{P_{CSM}}$	$\frac{N_{FEA}}{N_{Rd,EC9}}$	$\frac{P_{CSM}}{N_{Rd,EC9}}$	$\frac{P_{DSM}}{N_{Rd,EC9}}$	$\frac{N_{FEA}}{P_{DSM}}$
Q5	1.04	1.62	1.55	1.51	1.08
K5	1.08	1.42	1.31	1.26	1.12
S5	1.13	1.48	1.31	1.26	1.17
S6	1.51	4.81	3.19	2.50	1.92
Cross-Section	**CSM-FEA**	**FEA-EC9**	**CSM-EC9**	**DSM-EC9**	**FEA-DSM**
Q5	−4%	62%	55%	51%	8%
K5	−8%	42%	31%	26%	12%
S5	−13%	48%	31%	26%	17%
S6	−51%	381%	219%	150%	92%

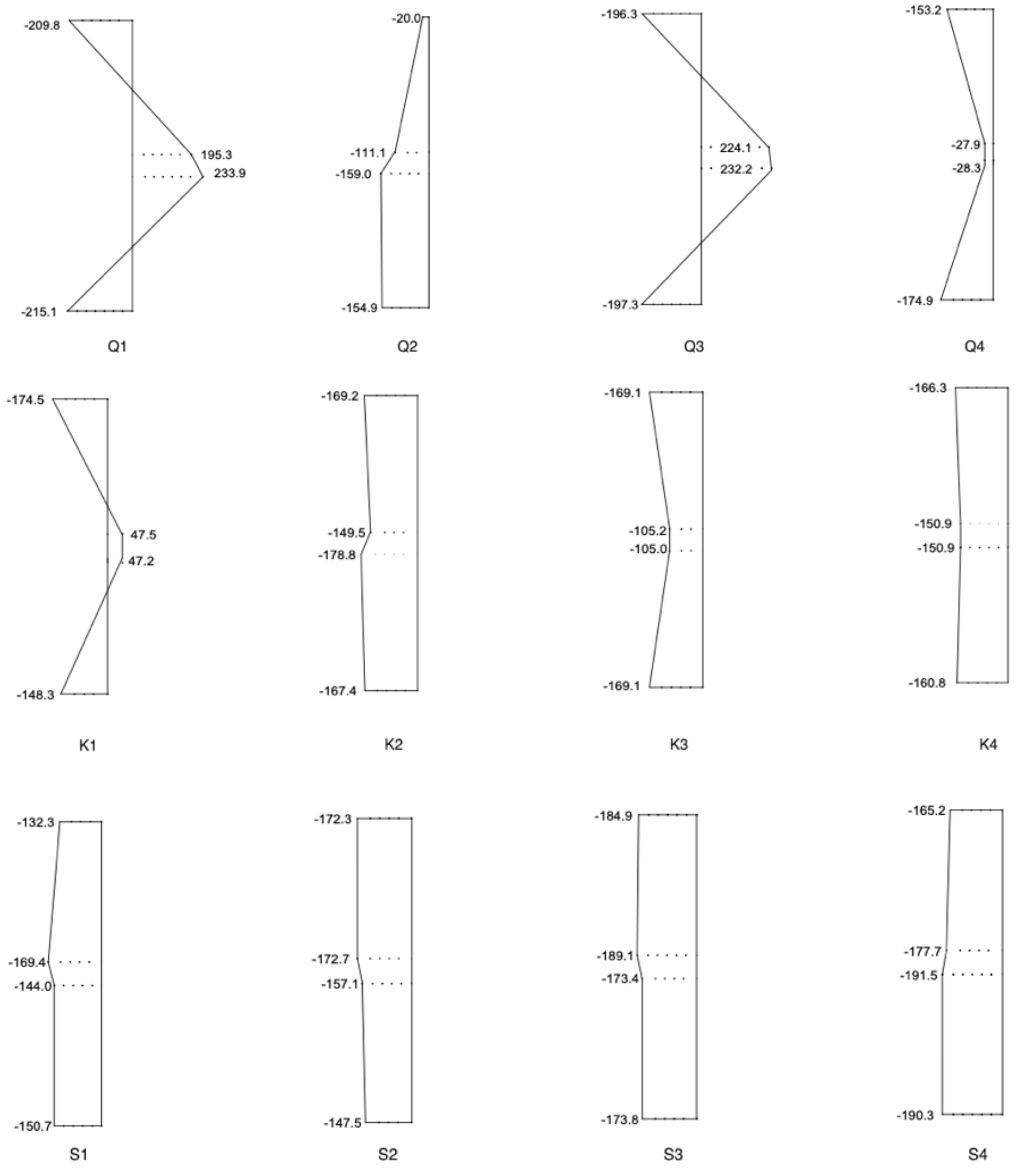

Figure A1. Cross-sectional stress distribution diagrams at maximum load for the web of each column type.

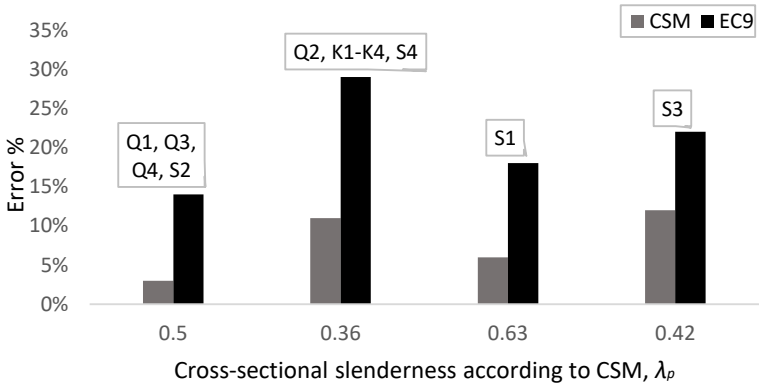

(**a**)

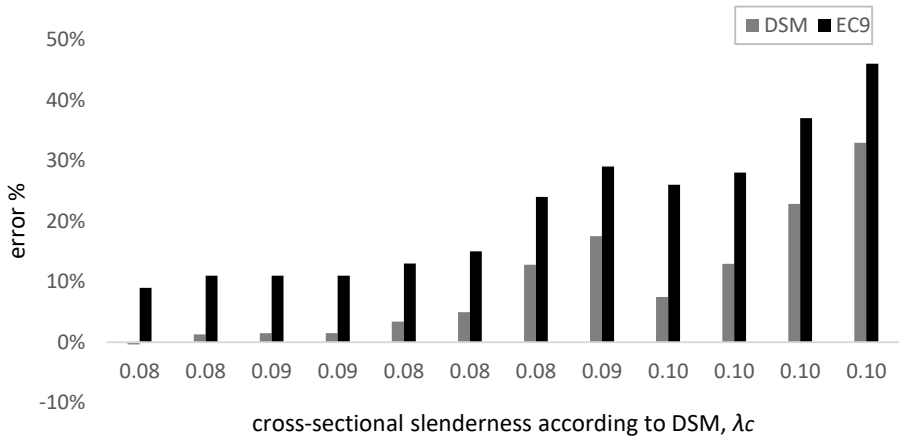

(**b**)

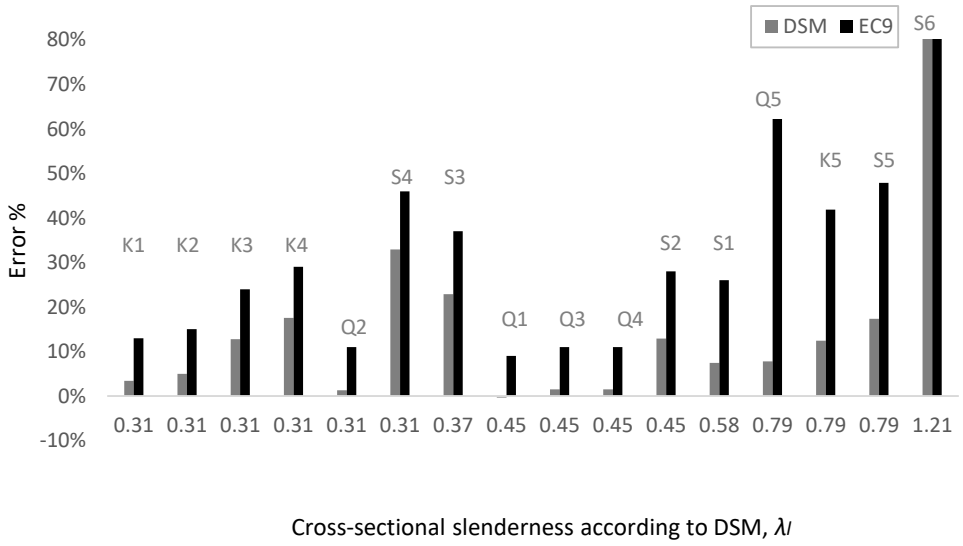

(**c**)

Figure A2. (**a**) Stocky cross-sections: error (percentage of difference among prediction value and FEA results). Predictions include EC9 and CSM. (**b**) Stocky cross-sections: error (percentage of difference among prediction value and FEA results). Predictions include EC9 and DSM. (**c**) All cross-sections: error (percentage of difference among prediction value and FEA results). Predictions include EC9 and DSM.

References

1. Tsavdaridis, K.D.; Efthymiou, E.; Adugu, A.; Hughes, J.A. Application of Structural Topology Optimisation in aluminium cross-sectional design. *Thin-Walled Struct.* **2019**, *139*, 372–388. [CrossRef]
2. Bendsoe, M.P.; Sigmund, O. *Topology Optimisation*; Springer: Berlin/Heidelberg, Germany, 2004.
3. Mei, L.; Wang, Q. Structural Optimization in Civil Engineering: A Literature Review. *Buildings* **2021**, *11*, 66. [CrossRef]
4. Rozvany, G. Aims, scope, methods, history and unified terminology of computer-aided topology optimization in structural mechanics. *Struct. Multidisc. Optim.* **2021**, *21*, 90–108. [CrossRef]
5. Haber, R.B.; Jog, C.S.; Bendsoe, M.P. A new approach to variable-topology shape design using a constraint on perimeter. *Struct. Optim.* **1996**, *11*, 1–12. [CrossRef]
6. Kim, Y.Y.; Kim, T.S. Topology optimization of beam cross sections. *Int. J. Solids Struct.* **2000**, *37*, 477–493. [CrossRef]
7. Gardner, L. The continuous strength method. *Proc. Inst. Civ. Eng.-Struct. Build.* **2008**, *161*, 127–133. [CrossRef]
8. Gardner, L.; Theofanous, M. Discrete and continuous treatment of local buckling in stainless steel elements. *J. Constr. Steel Res.* **2008**, *64*, 1207–1216. [CrossRef]
9. Afshan, S.; Gardner, L. The continuous strength method for structural stainless steel design. *Thin-Walled Struct.* **2013**, *68*, 42–49. [CrossRef]
10. Gardner, L.; Wang, F.; Liew, A. Influence of strain hardening on the behaviour and design of steel structures. *Int. J. Struct. Stab. Dyn.* **2011**, *11*, 855–875. [CrossRef]
11. Theofanous, M.; Propsert, T.; Knobloch, M.; Gardner, L. The continuous strength method for steel cross-section design at elevated temperatures. *Thin-Walled Struct.* **2016**, *98*, 94–102. [CrossRef]
12. Yun, X.; Xiang, L.; Gardner, L. The continuous strength method for the design of cold-formed steel non-slender tubular cross-sections. *Eng. Struct.* **2018**, *175*, 549–564. [CrossRef]
13. Buchanan, C.; Gardner, L.; Liew, A. The continuous strength method for the design of circular hollow sections. *J. Constr. Steel Res.* **2015**, *118*, 207–216. [CrossRef]
14. *BS EN 1999-1-1*; Eurocode 9: Design of Aluminium Structures-Part 1-1: General Structural Rules. European Union: Brussels, Belgium, 2009. Available online: https://www.phd.eng.br/wp-content/uploads/2014/11/en.1999.1.1.2007.pdf (accessed on 10 September 2022).
15. Ashraf, M.; Young, B. Design formulations for non-welded and welded aluminium columns using Continuous Strength Method. *Eng. Struct.* **2011**, *33*, 3197–3207. [CrossRef]
16. Su, M.-N.; Young, B.; Gardner, L. The continuous strength method for the design of aluminium alloy structural elements. *Eng. Struct.* **2016**, *122*, 338–348. [CrossRef]
17. Su, M.-N.; Young, B.; Gardner, L. Testing and Design of Aluminum Alloy Cross Sections in Compression. *J. Struct. Eng.* **2014**, *140*, 04014047. [CrossRef]
18. Su, M.-N.; Young, B.; Gardner, L. Deformation-based design of aluminium alloy beams. *Eng. Struct.* **2014**, *80*, 339–349. [CrossRef]
19. Su, M.N.; Young, B.; Gardner, L. Classification of aluminium alloy cross-sections. *Eng. Struct.* **2017**, *141*, 29–40. [CrossRef]
20. Ampatzis, A.T.; Psomiadis, V.G.; Efthymiou, E. Plastic collapse of hardening spatial aluminium frames: A novel shakedown-based approach. *Eng. Struct.* **2017**, *151*, 724–744. [CrossRef]
21. Georgantzia, E.; Gkantou, M.; Kamaris, G.S.; Kansara, K.D. Ultimate response and plastic design of aluminium alloy continuous beams. *Structures* **2022**, *39*, 175–193. [CrossRef]
22. Schafer, B.W.; Peköz, T. Direct Strength Prediction of Cold-Formed Steel Members using Numerical Elastic Buckling Solutions. In Proceedings of the 14th International Specialty Conference on Cold-Formed Steel Structures, St. Louis, MO, USA, 15–16 October 1998.
23. Schafer, B.W. Distortional buckling of cold-formed steel columns. In *Final Report to the American Iron and Steel Institute*; American Iron and Steel Institute: Washington, DC, USA, 2000.
24. Schafer, B.W. Progress on the direct strength method. In Proceedings of the 16th International Specialty Conference on Cold-Formed Steel Structures, Orlando, FL, USA, 17–18 October 2002; pp. 647–662.
25. Schafer, B.W. Review: The Direct Strength Method of cold-formed steel member design. *J. Constr. Steel Res.* **2008**, *64*, 766–778. [CrossRef]
26. American Iron and Steel Institute. *North American Specification for the Design of Cold-Formed Steel Structural Members*; American Iron and Steel Institute: Washington, DC, USA, 2012.
27. American Iron and Steel Institute. *Supplement 2004 to the North American Specification for the Design of Cold-Formed Steel Structural Members*, 2001th ed.; AISI-Specifications for the Design of Cold-Formed Steel Structural Members; 131; American Iron and Steel Institute: Washington, DC, USA, 2005.
28. *AS/NZS 4600*; Cold-Formed Steel Structures. Standards Australia: Sydney, Australia, 2018.
29. Zhu, J.H.; Young, B. Aluminium alloy tubular columns–Part II: Parametric study and design using direct strength method. *Thin-Walled Struct.* **2006**, *44*, 969–985. [CrossRef]
30. Zhu, J.H.; Li, Z.Q.; Su, M.N.; Young, B. Behaviour of Aluminium Alloy Plain and Lipped Channel Columns. *Thin-Walled Struct.* **2019**, *135*, 306–316. [CrossRef]
31. Dassault Systèmes, D. ABAQUS 6.14 Analysis User's Manual. 2014. Available online: http://130.149.89.49:2080/v6.14/pdf_books/ANALYSIS_4.pdf (accessed on 10 September 2022).

32. Dinis, P.; Camotim, D. Post-buckling behaviour and strength of cold-formed steel lipped channel columns experiencing distortional/global interaction. *Comput. Struct.* **2011**, *89*, 422–434. [CrossRef]
33. Landesmann, A.; Camotim, D.; Basaglia, C. Distortional Post-Buckling Behaviour and Strength of Cold-Formed Steel Columns: How does the Cross-Section Geometry Affect it? In Proceedings of the Annual Stability Conference, Structural Stability Research Council, St. Louis, MO, USA, 16–20 April 2013.
34. Soimoiris, G. Buckling of Frames and Columns with Initial Imperfection. Master's Thesis, National Technical University of Athens, Department of Computational Mechanics, Athens, Greece, 2011.
35. Höglund, T. Design of Members, Royal Institute of Technology. In *TALAT–Training in Aluminium Technologies 2301*; European Aluminium Association: Stockholm, Sweden, 2008.
36. Seif, M.; Schafer, B.W. Local buckling of structural steel shapes. *J. Constr. Steel Res.* **2010**, *66*, 1232–1247. [CrossRef]
37. Zhu, J.H.; Young, B. Numerical investigation and design of aluminium alloy circular hollow section columns. *Thin-Walled Struct.* **2008**, *46*, 1437–1449. [CrossRef]
38. Zhu, J.H.; Young, B. Tests and Design of Aluminium Alloy Compression Members. *J. Struct. Eng. ASCE* **2006**, *132*, 1096–1107. [CrossRef]
39. Gardner, L.; Fieber, A.; Macorini, L. Formulae for Calculating Elastic Local Buckling Stresses of Full Structural Cross-Sections. *Structures* **2019**, *17*, 2–20. [CrossRef]
40. Georgantzia, E.; Gkantou, M.; Kamaris, G.S. Numerical Modelling and Design of Aluminium Alloy Angles under Uniform Compression. *Civil. Eng.* **2021**, *2*, 632–651. [CrossRef]